Nigerian Journal of Technology (NIJOTECH)
Vol. 44, No. 4, December, 2025, pp. 576- 589
www.nijotech.com

Print ISSN: 0331-8443
Electronic ISSN: 2467-8821
https://doi.org/10.4314/njt.2025.5580

OPTIMIZATION OF FCA AND MIG WELDING PARAMETERS FOR AISI-1045 STEEL

AUTHORS:
C. C. Irechukwu[1], S. A. Lawal[1], I. O. Sadiq[1], A. A. Abdullahi[1], and J. Abutu[2*]

AFFILIATIONS:
[1]Department of Mechanical Engineering, Federal University of Technology, Minna, NIGERIA
[2]Department of Mechanical Engineering, Taraba State University, Jalingo, NIGERIA

***CORRESPONDING AUTHOR:**
Email:abutu.joseph@tsuniversity.edu.ng

ARTICLE HISTORY:
Received: September 06, 2025.
Revised: December 02, 2025.
Accepted: December 04, 2025.
Published: January 03, 2026

KEYWORDS:
Welding; FCAW, MIGW, grey relational analysis; Taguchi; welding parameters
.

ARTICLE INCLUDES:
Peer review

DATA AVAILABILITY:
On request from author(s)

EDITORS:
Ozoemena Ani

FUNDING:
None

Abstract

Welding is a vital industrial process for joining metals and thermoplastics, with Metal Inert Gas (MIG) and Flux Cored Arc (FCA) welding widely used due to their versatility and effectiveness. This study optimized FCA and MIG welding parameters for AISI 1045 alloy steel using Response Surface Methodology (RSM) via Central Composite Design (CCD) $L_{20}(5)^3$ in Minitab 20. The parent material and weldments were characterized through standard testing methods. X-ray fluorescence (XRF) analysis confirmed the material as galvanized medium-carbon steel containing 0.376% carbon and 22–25% iron, while revealing a crystalline structure with features indicating crystal size and possible defects. Mechanical testing showed UTS values for welds were generally lower than the base metal, high joint efficiencies confirmed good bonding. Also, optimal conditions for hardness (FCAW: 4.6 kgm/s, 73.2 A, 28 mm; MIG: 8 kgm/s, 73.2 A, 24.6 mm), UTS (FCAW: 10 kgm/s, 73.2 A, 26 mm; MIG: 8 kgm/s, 73.2 A, 24.6 mm), and impact strength (MIG: 6 kgm/s, 106.8 A, 26 mm), with gas flow rate as the dominant factor and refined microstructures confirming superior weld quality and bonding. Both welds were free from porosity and cracks, underscoring the importance of parameter optimization for superior weld quality and mechanical performance.

1.0 INTRODUCTION

Welding is an essential joining technique that has played a vital role in the advancement of modern industries and the growth of nations. It entails bonding materials most commonly metals or thermoplastics by applying heat, pressure, or both, to create strong, durable connections that ensure structural strength and reliable performance. This process is crucial in various sectors such as automotive, aerospace, shipbuilding, and construction, owing to its flexibility and capability to deliver high-quality joints that comply with rigorous safety and performance requirements. [1-2]. The versatility of welding is demonstrated by its wide range of applications, addressing diverse manufacturing challenges from assembling intricate components to building large-scale infrastructure. Various welding techniques, including arc welding,

HOW TO CITE:
Irechukwu, C. C., Lawal, S. A., Sadiq, I. O., Abdullahi, A. A. and Abutu, J. "Optimization of FCA and MIG Welding Parameters for AISI-1045 Steel", *Nigerian Journal of Technology*, 2025. 44(4), pp. 576- 589. https://doi.org/10.4314/njt.2025.5580

resistance welding, laser welding, and friction stir welding, are customized to suit specific materials and purposes, ensuring maximum performance and longevity. These methods are fundamental to contemporary manufacturing, facilitating the construction of complex assemblies, increasing product durability, and boosting industrial productivity [2]. As Kearns [3] emphasizes, welding serves as a cornerstone in manufacturing, facilitating the production of essential components such as automotive bodies, large metal structures, pressure vessels, spacecraft, and aircraft. Moreover, ongoing research in welding science is dedicated to optimizing techniques, improving mechanical properties, and increasing efficiency in both semi-automated and fully automated manufacturing environments. Messler [4] highlights welding's foundational role in "binding the world together," noting that advancements in welding technology are crucial for meeting the evolving demands of modern industry.

Among the various welding methods, Metal Inert Gas Welding (MIG) and Flux Cored Arc Welding (FCAW) are particularly prominent due to their adaptability and widespread industrial use [5]. FCAW utilizes a tubular wire electrode filled with flux, which generates a shielding gas to protect the weld pool from atmospheric contamination [6]. This method is especially valued for its high deposition rates and suitability for welding thick materials, making it a preferred choice in heavy fabrication and shipbuilding [2]. Conversely, MIG welding employs a solid wire electrode and uses external shielding gases such as argon or carbon dioxide to prevent oxidation and contamination of the weld [5, 7]. This method is well-known for its ease of automation, clean weld finishes, and suitability for various metals such as aluminum and stainless steel. FCAW and MIG are widely employed in sectors like aerospace, shipbuilding, and automotive manufacturing because they consistently deliver high-quality and dependable weld [2]. Despite their advantages, FCAW and MIG welding processes are not without challenges. For instance, MIG welding can induce internal stresses due to thermal expansion and contraction, potentially leading to distortion or cracking. FCAW welds, meanwhile, are susceptible to defects such as porosity and slag inclusions, which can compromise the mechanical properties of the joint. Addressing these issues requires careful optimization of key welding parameters including current, voltage, gas flow rate, and electrode extension to improve weld quality and mechanical properties such as tensile strength, hardness, and impact resistance [3-4]. Numerous studies have employed experimental design techniques to systematically optimize welding parameters and enhance weld quality. For example, Vijayavel et al. [8] focused on maximizing the tensile strength of MIG-welded AISI 1050 carbon steel by analyzing the effects of welding current, gas flow rate, voltage, and wire speed using a four-factor, three-level composite design. Similarly, Ajit et al. [9] developed predictive models for AISI 1040 steel, identifying optimal voltage, current, and gas flow rates to enhance yield strength. Also, for specialized alloys such as Hastelloy C276, Raja et al. [10] investigated the relationship between MIG welding parameters (current, voltage, gas flow) and microstructure evolution, demonstrating the utility of Response Surface Methodology RSM) in controlling weld integrity and mechanical performance. Doniawi et al. [11] optimized argon-CO_2 gas mixtures and current for gas metal arc welding (GMAW) of St 52 steel, achieving high tensile strength through models validated by Analysis of Variance (ANOVA). Izzatul et al. [12] further highlighted the influence of welding current and arc voltage on penetration depth and hardness (in mild steel, correlating microstructural changes with parameter adjustments. In the context of FCAW, Kashif and Anwar [13] analyzed the effects of current, wire feed rate, and contact tip distance to optimize strength, bead geometry, and deposition rates in medium alloy steel, using desirability functions to identify ideal weld conditions. Rayindra and Rajesh [14] extended these principles to MIG welding of AISI 316 steel, prioritizing parameters such as voltage, speed, and gas flow to enhance tensile properties and minimize defects.

Also, Recent studies have optimized welding parameters for AISI 1045 steel using advanced multi-objective methods and characterization techniques. Igwe et al. [24-27] investigated the machinability, surface quality, and corrosion behaviour of additively manufactured AlSi10Mg and rice husk ash reinforced aluminum using factorial analysis, Taguchi-Grey relational optimization, and experimental SLM/LPBF studies, identifying optimal parameters (such as laser power: 250 W, scan speed: 2000 mm/s, hatch space: 150 µm) that yielded as-built hardness of ~125 HV, porosity of 3%, and improved surface roughness and corrosion resistance, with microstructural analysis confirming refined grains and enhanced mechanical properties. In addition Van et al. [28] applied entropy, modified grey wolf optimizer (MGWO), and MABAC to

https://doi.org/10.4314/njt.2025.5580

identify optimal GMAW parameters (137 A, 23 V, 12 L/min gas flow, 12 mm electrode extension), improving tensile strength and elongation while reducing energy consumption. Lawong et al. [29] introduced a multi-response approach for robotic GMAW, highlighting tailored parameters for dissimilar joints. Jawad et al. [30] examined GTAW parameter effects on microstructure and mechanical properties. Marimuthu et al. [31] used particle swarm optimization to minimize residual stresses, demonstrating the effectiveness of intelligent algorithms in balancing weld quality objectives. These works collectively emphasize data-driven, multi-response optimization and advanced microstructural analysis for enhancing AISI 1045 weld quality.

Therefore, building on these foundational studies, the present research aims to optimize FCAW and MIG welding parameters for AISI 1045 alloy steel using advanced statistical and experimental techniques, specifically Response Surface Methodology (RSM) and Grey Relational Analysis (GRA). By systematically comparing the performance of these two welding techniques through rigorous experimental design and statistical analysis, the study seeks to enhance weld quality, improve mechanical properties, and ensure greater industrial efficiency. Therefore, welding remains a cornerstone of modern manufacturing, with ongoing research focused on optimizing processes for improved quality and performance. The integration of advanced experimental design and statistical analysis methods continues to drive innovation, ensuring that welding technologies evolve to meet the complex demands of contemporary industry [2-4, 9]

2.0 MATERIALS AND METHODS

2.1 Materials

In this study, Metal Inert Gas (MIG) welding employed a copper-coated carbon steel wire (AFROX MIG 6000) as the consumable electrode, shielded by argon gas to protect the weld pool from contamination. This electrode was chosen for its cost-effectiveness, availability, adaptability to all welding positions, and suitability for thin sheet metal applications due to its shallow penetration. Also, Flux-Cored Arc Welding (FCAW) utilized a SUPERCORE 71 flux-cored wire (ISO 9001 certified), which contained flux within its core to shield the weld during melting. Both electrodes, were locally sourced from a commercial supplier in Kaduna, Nigeria. In addition, Argon was used as shielding gases in this study to protect the weld pool from atmospheric contamination in during MIG and FCAW processes, while solenoid valves regulate gas flow, welding guns and torches ensure precise electrode feeding and arc control while galvanized AISI 1045 alloy steel was used as the experimental workpiece,

2.2 Methods

2.2.1 Characterisation of parent material

Locally sourced parent materials used for welding were characterized using X-ray diffraction (XRD) to determine their crystallographic structure and X-ray fluorescence (XRF) to establish their elemental chemical composition, providing a comprehensive understanding of their properties. Experiments were conducted following standard testing procedures as stipulated in the literature.

2.2.2 Experimental design

Experimental design was carried out in accordance with the Response Surface Methodology (RSM) – Central Composite Design (CCD) $L_{20}(5)^3$ method using Minitab 20 statistical software. The factor levels of welding parameters are shown in Table 1, while the Taguchi orthogonal array and design matrix are also presented in Table 1. The parameter ranges selected, along with the current values (73.2 A and 106.8 A), gas flow rate values (4.6 and 11.4 kgm/s), and electrode extension values (24.6 and 31.4 mm) as axial points in the Central Composite Design, allow exploration beyond the cubic points, giving a wider design space that accounts for potential nonlinear effects. These axial points typically extend ±α from the center points (8 kgm/s, 90 A, and 28 mm) to provide better model fitting and enhance robustness in identifying optimal welding conditions.

Table 1: Factor levels of welding parameters

	Cubic points		Axial points		Center Point
Welding parameter	-1	+1	-α	+ α	0
Gas Flow Rate (kgm/s)	6	10	4.6	11.4	8
Arc current (Amp)	80	100	73.2	106.8	90
Electrode extension (mm)	26	30	24.6	31.4	28

https://doi.org/10.4314/njt.2025.5580
http://creativecommons.org/licenses/by-nc-nd/4.0/

2.2.3 Experimental procedure

The MIG welding in this study involved striking an arc between a wire electrode and parent material, melting both to form a weld pool [15]. The wire served as heat source and filler, fed through a copper contact tube carrying the welding current.

Table 2: CCD $L_{20}(5)^3$ experimental design matrix

Run	Gas Flow Rate (kgm/s)	Arc Current (Amp)	Electrode extension (mm)
1	6.0	80.0	26.0
2	10.0	80.0	26.0
3	6.0	100.0	26.0
4	10.0	100.0	26.0
5	6.0	80.0	30.0
6	10.0	80.0	30.0
7	6.0	100.0	30.0
8	10.0	100.0	30.0
9	4.6	90.0	28.0
10	11.4	90.0	28.0
11	8.0	73.2	28.0
12	8.0	106.8	28.0
13	8.0	90.0	24.6
14	8.0	90.0	31.4
15	8.0	90.0	28.0
16	8.0	90.0	28.0
17	8.0	90.0	28.0
18	8.0	90.0	28.0
19	8.0	90.0	28.0
20	8.0	90.0	28.0

Shielding gas protected the weld pool, chosen based on material and application, with the welding torch moving along the joint. FCA welding, using similar equipment and a continuous wire-fed electrode, was performed with shielding gas in this research. Both methods had wire feed rate and arc length controlled by the power source, while travel speed and wire position were manually adjusted. Stainless steel samples (120 x 120 x 1 mm) were cut and cleaned with acetone before welding. Mechanical properties of the welds were tested according to ASTM E8, E10, and E23 standards.

2.2.3 Characterization of weldments

Mechanical properties

Tensile strength testing of AISI 1045 steel weldments was performed using three specimens per tensile testing condition, in accordance with ASTM E8 standard, on a 50 kN Instron Universal Tensile Machine. Ultimate tensile stress (Equation 1) and joint efficiency (Equation 2) were calculated from maximum force measurements and comparisons with the base material. Also, hardness tests were conducted using a 5 kg Vickers hardness tester in compliance with ASTM E10. Twenty mirror-polished samples, each measuring 120 mm × 120 mm × 1 mm, were tested. Nine indentations were made across the weld zones, with a 2-second dwell time, and the results were averaged to determine nugget zone hardness. In addition, charpy impact tests were performed using a Galdabani V92Q machine, following ASTM E23. Twenty coupons, each measuring 120 mm × 120 mm × 1 mm, with 45° notches (0.25 mm radius, 2 mm depth) positioned perpendicular to the weld, were used. Three replicate tests were averaged per sample to determine impact strength (Equation 3).

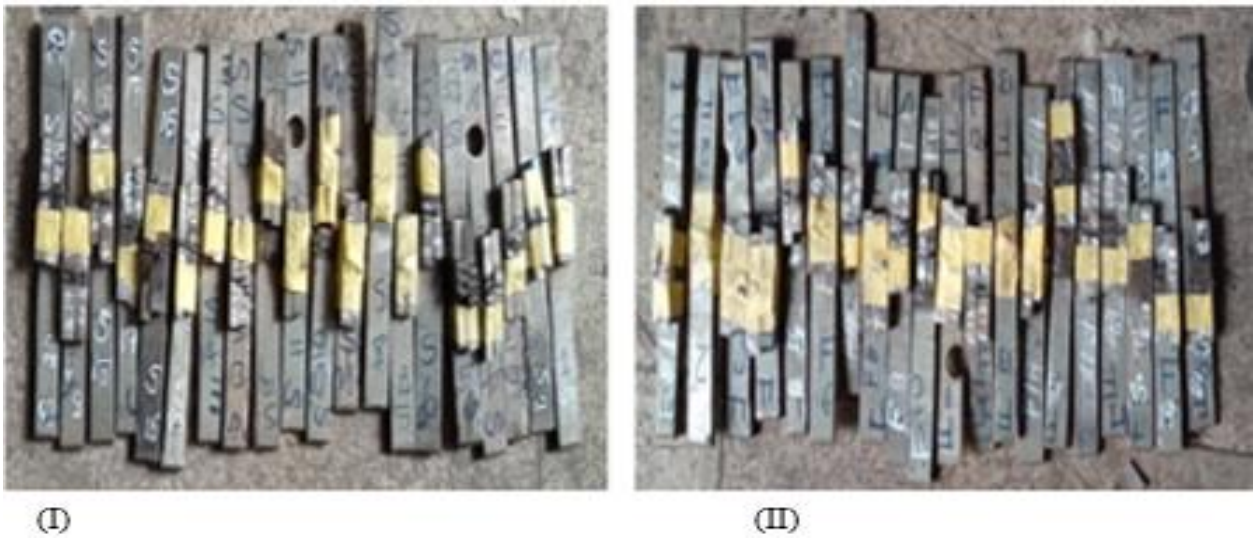

Figure 1: weldment (i) FCAW and (ii) MIGW

Ultimate tensile Stress $(\sigma) = \frac{\text{Maximum Force (Pmax)}}{\text{cross-sectional area (A)}}$ (1)

Joint efficiency (η) = $\frac{UTS\ of\ welded\ joint}{UTS\ of\ base\ material}$ x 100 % (2)

Impact strenght (I_s) = $\frac{\text{Absorbed energy}(E_a)}{Thickness\ of\ specimen(t)}$ (3)

Microstructural characterization

The inner and microstructures of optimized weldments were analyzed using an optical microscope at various magnifications and a Scanning Electron Microscope (SEM) at the Nigerian Building and Road Research Institute (NBRRI) in Abuja-Nigeria, following a detailed preparation process involving polishing, grinding to a mirror finish, cleaning with acetone, and selecting one sample each from FCAW and MIGW techniques

2.2.4 Analysis of experimental results

Mechanical test results (hardness, tensile, impact) were analyzed using Signal to Noise (SN) ratio and ANOVA to optimize responses and assess each factor's contribution to tensile strength, impact energy, and hardness in FCAW and MIGW samples. SN ratios used the larger-the-better criterion (Equation 4), and ANOVA sum of squares were calculated via Equation 5.

$$S/N(\eta) - 10\log\frac{1}{n}\left(\sum_{i-1}^{n}\frac{1}{y_i^2}\right) \quad (4)$$

$$Sum\ of\ square\ (total) = \sum y_i^{\,2} - \frac{1}{n}(\sum y_i)^2$$

(i = 1, 2, 3....., 20) (5)

Where n = number of observation and r = response value

2.2.5 Multi-response optimization

Multi-response optimization of experimental data was conducted using Grey Relational Analysis (GRA), following the methodology outlined by Abutu et al. [17] and Irechukwu et al. [18], which involves calculating the Grey Relational Generation (GRG) using Equation 6 from SN ratio values using larger-the-better attributes, determining the Grey Relational Coefficient (GRC) using Equation 7, computing the Grey Relational Grade (GR-grade) by utilizing Equation 8, and identifying optimal conditions for single response optimization.

$$\text{Larger}-the\,better\ attributes\,(y_{ij}) = \frac{p_{ij} - \underline{p_i}}{\overline{p_i} - p_j} \quad (i = 1, 2, 3, 4\ldots. u \text{ and } j = 1, 2, 3, 4\ldots. v) \quad (6)$$

Where, $p_i = p_{i1}, p_{i2}, \ldots, p_{ij}, \ldots, p_{in}$), p_{ij}= the performance value of attribute j of alternative i and $\overline{p_i} = \max\{p_{ij}, i = 1, 2, \ldots, u\}$ and $\underline{p_i} = \min\{p_{ij}, i = 1, 2, \ldots, v\}$.

$$GRC\,(GRC_{oj}, GRC_{ij}) = \frac{\tau_{\min} + E\tau_{\max}}{\tau_{ij} + E\tau_{\max}} \quad (7)$$

Where, E is the distinguishing coefficient. Abutu et al. [17] and Irechukwu et al. [18], reported that 0.5 is the widely accepted value of E.

$\tau_{ij} = p_0 j - pij$, $\tau\Delta_{\min} = \min(\tau_{ij}, i = 1, 2, \ldots, u; j = 1, 2, \ldots, v)$ and $\tau_{\max} = \max(\Delta_{ij}, i = 1, 2, \ldots, u; j = 1, 2, \ldots, v)$,

$$\text{GR-grade} = \frac{Individual\ \ GRC}{Number\ \ of\ \ \text{exp}erimental\ responses} \quad (8)$$

3.0 RESULTS AND DISCUSSION

3.1 Characterisation of Parent Material

The X-ray Fluorescence (XRF of the parent materials was presented in Table 3. It can be observed that the carbon content of the sample tested was 0.376% and iron content of <25-22%. Medium-carbon steel has a carbon content that falls between 0.3%-0.6%. Increased carbon means increased hardness, tensile strength, decreased ductility and more difficult machining. Hence, the sample tested was a Galvanised medium-carbon steel. Also, X-ray diffraction results which determine the crystallographic structure, chemical composition and physical properties of the parent material was presented in Figure 2.The result of x-ray diffraction (XRD) analysis presented in Figure 2 represent the intensity of the signal for various angles of

diffraction at their respective two theta positions correspond to a certain spacing between the crystals of atoms in the samples, determined by the angle of diffraction from the incident x-ray beam sent into the sample. The intensity of the peaks was related to the amount of molecular in that phase or with that spacing. The greater the intensity of the peak, the greater the amount of the crystals or molecular with that district spacing. The width of the peaks was inversely proportional to the crystal size [22]. A thinner peak corresponds to a bigger crystal. A broader peak means that there may be a smaller crystal defect in the crystalline structure or that the sample might be amorphous in nature a solid lacking perfect crystallinity [23]. For smaller samples, the pattern determined using XRD analysis can be used to determine a sample composition. The sample composition was crystalline in nature.

Table 3: Chemical composition of AISI 1045 alloy steel.

Sample Elements	First Spark (%)	Second Spark (%)	Average Spark (%)	Sample Elements	First Spark (%)	Second Spark (%)	Average Spark (%)
C	0.300	0.452	0.376	**Ti**	0.025	0.032	0.028
AL	0.011	0.017	0.014	**Zn**	>0.036	>0.036	>0.036
Mg	0.012	0.014	0.013	**S**	0.018	0.035	0.026
Zr	0.0015	0.0031	0.0022	**Nb**	0.027	0.031	0.029
Si	0.066	0.090	0.078	**As**	0.019	0.027	0.023
Cu	0.026	0.025	0.026	**Cr**	0.016	0.030	6.023
B	0.0037	0.0062	0.0050	**V**	0.017	0.021	0.019
La	0.032	0.046	0.039	**Bi**	0.0028	0.0061	0.0044
Mn	0.171	0.149	0.160	**Ni**	0.069	0.094	0.084
Sco	0.028	0.040	0.034	**W**	0.023	0.056	0.040
Sn	0.011	0.015	0.013	**Ca**	0.0038	0.0064	0.0051
Fe	<26.28	<24.16	<25.22	**Mo**	0.085	0.119	0.102
P	0.0084	0.016	0.012	**Pb**	0.014	0.033	0.023
				Ce	0.031	0.045	0.033

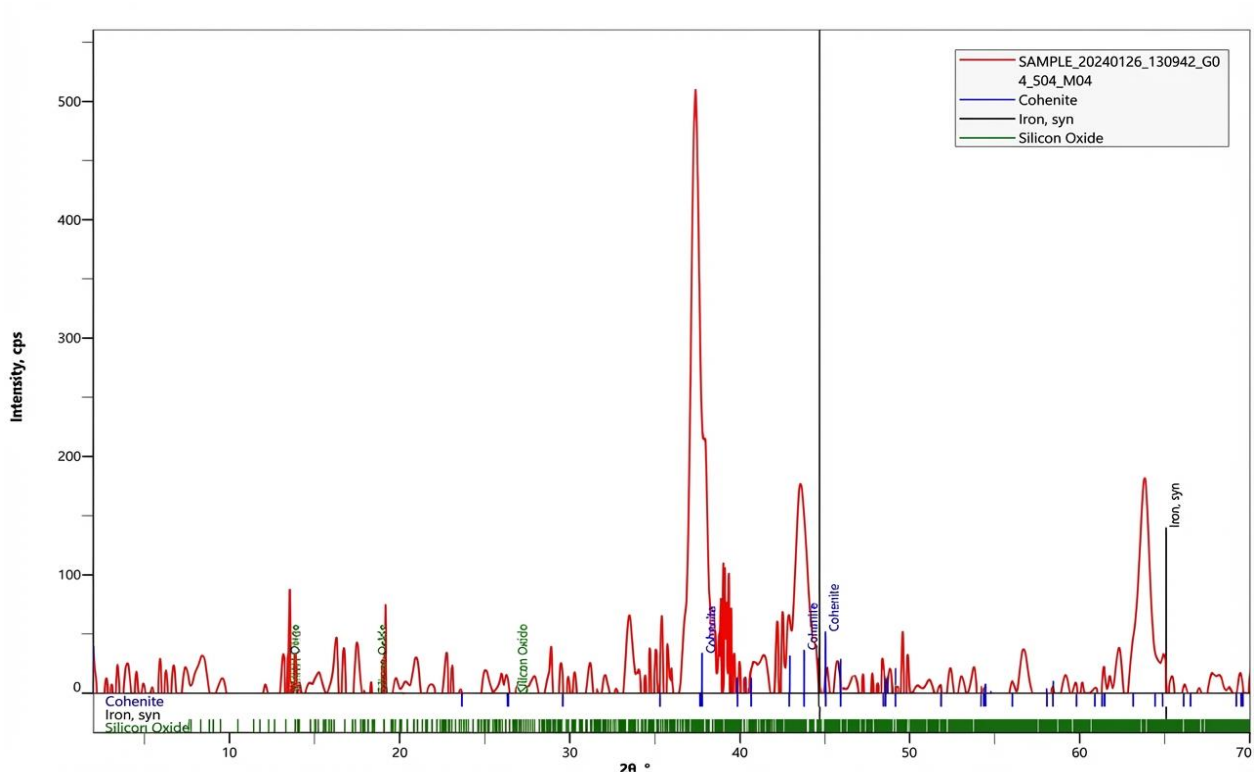

Figure 2: Graph of result sample tested for x-ray diffraction.

https://doi.org/10.4314/njt.2025.5580
http://creativecommons.org/licenses/by-nc-nd/4.0/

3.2 Experimental Results

The average values from the characterization of Flux-Cored Arc (FCA) and Metal Inert Gas (MIG) weldments, along with their joint efficiencies, are summarized in Tables 4 while the Signal to noise (SN) ratio values for weldments obtained from FCAW and MIGW is presented in Table 5. The results shown in Table 4 showed that tensile strength tests on the base metal yielded a UTS of 642.44 MPa, closely matching the 639.8 MPa reported by Singh et al. [21] for galvanized medium carbon steel. For FCAW, average hardness ranged from 104.67 to 199.22 HV, UTS from 339.54 MPa (52.85% joint efficiency) to 632.72 MPa (98.49% joint efficiency), and impact strength from 4.74 to 26.59 J/mm, with property variations linked to changes in welding parameters and improvements attributed to enhanced grain refinement and mixing at moderate gas flow rates.

Although the UTS values were generally lower than the parent material, the high joint efficiencies indicate good bonding properties. Similarly, for MIGW, average hardness ranged from 74.22 to 202.11 HV, UTS from 98.94 MPa (15.40% joint efficiency) to 640.43 MPa (99.69% joint efficiency), and impact strength from 5.25 to 16.59 J/mm, with property changes also reflecting the influence of welding parameters and improvements due to better grain refinement and mixing. Despite UTS values being below that of the base metal, substantial joint efficiencies confirm strong weld bonding.

Table 4: Experimental results of sample characterization (FCAW and MIGW)

Runs	MIGW				FCAW			
	Hardness (HVN)	UTS (MPa)	Impact Strength (J/mm)	Joint efficiency (%)	Hardness (HVN)	UTS (MPa)	Impact Strength (J/mm)	Joint efficiency (%)
1	145.67	463.00	16.59	72.07	189.00	609.65	13.30	94.90
2	115.44	332.96	5.250	51.83	168.63	535.65	12.18	83.38
3	184.89	600.16	8.360	93.42	142.38	462.49	26.59	71.99
4	163.22	512.35	14.16	79.75	192.25	632.72	11.84	98.49
5	170.44	517.13	9.450	80.49	183.44	593.04	9.200	92.31
6	177.33	572.81	8.360	89.16	182.56	586.26	17.61	91.26
7	112.00	362.39	9.270	56.41	104.67	339.54	9.950	52.85
8	185.67	580.09	8.430	90.29	189.11	623.83	9.130	97.10
9	99.33	278.97	5.430	43.42	186.22	575.03	9.100	89.51
10	74.22	98.94	7.020	15.40	140.44	458.41	4.110	71.35
11	202.11	640.43	10.65	99.69	188.78	591.04	7.150	92.00
12	194.00	614.48	11.96	95.65	188.44	590.53	12.99	91.92
13	188.78	614.56	10.03	95.66	170.11	521.82	8.850	81.22
14	184.67	595.59	7.710	92.71	156.22	487.70	13.30	75.91
15	172.67	549.88	13.22	85.59	183.44	600.19	4.740	93.42
16	178.56	574.17	5.040	89.37	144.89	448.87	6.980	69.87
17	180.44	591.26	5.310	92.03	197.33	616.85	13.61	96.02

https://doi.org/10.4314/njt.2025.5580
http://creativecommons.org/licenses/by-nc-nd/4.0/

18	194.89	616.25	8.920	95.92	169.89	503.50	11.05	78.37
19	164.67	496.97	10.03	77.36	199.22	620.67	11.24	96.61
20	175.11	535.88	12.37	83.41	189.22	601.51	5.220	93.63

Table 5: Signal to noise ratio values for FCAW and MIGW

	FCAW			MIGW		
Runs	**Hardness (dB)**	**UTS (dB)**	**Impact Strength (dB)**	**Hardness (dB)**	**UTS (dB)**	**Impact Strength (dB)**
1	45.529	55.702	22.477	43.267	53.312	24.397
2	44.539	54.578	21.713	41.247	50.448	14.403
3	43.069	53.302	28.494	45.338	55.565	18.444
4	45.677	56.024	21.467	44.256	54.191	23.021
5	45.270	55.462	19.276	44.632	54.272	19.509
6	45.228	55.362	24.915	44.976	55.160	18.444
7	40.396	50.618	19.956	40.984	51.184	19.342
8	45.534	55.901	19.209	45.375	55.270	18.517
9	45.401	55.194	19.181	39.942	48.911	14.696
10	42.950	53.225	12.277	37.411	39.907	16.927
11	45.519	55.432	17.086	46.112	56.129	20.547
12	45.504	55.425	22.272	45.756	55.770	21.555
13	44.615	54.350	18.939	45.519	55.771	20.026
14	43.875	53.763	22.477	45.328	55.499	17.741
15	45.270	55.566	13.516	44.744	54.805	22.425
16	43.221	53.042	16.877	45.035	55.181	14.049
17	45.904	55.804	22.677	45.127	55.436	14.502
18	44.603	54.040	20.867	45.796	55.795	19.007
19	45.987	55.857	21.015	44.332	53.927	20.026
20	45.539	55.585	14.353	44.866	54.581	21.847

3.3 Analysis of Experimental Results

3.3.1 Analysis of variance

The combined analysis of ANOVA results for FCAW and MIG welding on AISI 1045 steel demonstrates that gas flow rate is the most influential parameter affecting weld quality across both processes. For FCAW, gas flow rate contributes 44.65% to hardness (Table 6) and 41.83% to UTS (Table 7) while electrode extension is dominant for impact strength (Table 8) at 36.97%. In MIG welding, gas flow rate's influence is even more pronounced, with contributions of 71.82% for hardness {Table 9) and 77.55% for UTS (Table 10), and it remains the leading factor for impact strength (Table 11) at 36.99%. Arc current and electrode extension have smaller but notable impacts in both methods, and the error (noise) is consistently low, indicating reliable experimental results. These findings align with earlier studies by Şeker et al. [32] and Abd-Rahman et al. [33] which also highlighted the critical role of gas flow rate in minimizing porosity and enhancing weld quality in both FCAW and MIG welding.

Table 6: ANOVA for hardness

Factor	DOF	SS	MS	F	P%
Gas Flow Rate (kgm/s)	4	4989	1247.25	57.83	44.65
Arc Current (Amp)	4	3452	863	40.015	30.89
Electrode extension (mm)	4	2582.6	645.65	29.94	23.11
Error	7	150.97	21.57		1.351

https://doi.org/10.4314/njt.2025.5580
http://creativecommons.org/licenses/by-nc-nd/4.0/

Total	19	11174.57	588.14		100

Table 7: ANOVA for UTS

Factor	DOF	SS	MS	F	P
Gas Flow Rate (kgm/s)	**4**	**48194**	**12048.50**	**15.78**	**41.83**
Arc Current (Amp)	**4**	**33637**	**8409.25**	**11.02**	**29.19**
Electrode extension (mm)	**4**	**28044**	**7011.00**	**9.18**	**24.34**
Error	**7**	**5343.737**	**763.39**		**4.64**
Total	**19**	**115218.7**	**6064.14**		**100.00**

Table 8: ANOVA for impact strength

Factor	DOF	SS	MS	F	P
GasFlow Rate (kgm/s)	4	151.00	37.75	24.24	31.64
Arc Current (Amp)	4	138.90	34.73	22.30	29.11
Electrode extension (mm)	4	176.40	44.10	28.32	36.97
Error	7	10.90	1.56		2.28
Total	19	477.20	25.12		100.00

Table 9: ANOVA for hardness

Factor	DOF	SS	MS	F	P
Gas Flow Rate (kgm/s)	4	17080	4270.0	27.05988663	71.82
Arc Current (Amp)	4	3492	873.0	5.532384317	14.68
Electrode extension (mm)	4	2105	526.3	3.334956754	8.85
Error	7	1104.587	157.8		4.64
Total	19	23781.59	1251.7		100.00

However, the current results diverge from some prior research that emphasized arc current or wire feed rate as the primary influences, likely due to differences in base material, process parameters, or experimental design [34]. Overall, both FCAW and MIG welding show that optimizing gas flow rate is essential for achieving high-quality welds in AISI 1045 steel, with gas flow rate emerging as the dominant factor for hardness and tensile strength, while electrode extension is particularly important for impact strength in FCAW.

Table 10: ANOVA for UTS

Factor	DOF	SS	MS	F	P
Gas Flow Rate (kgm/s)	4	283228.00	70807.00	39.62	77.55
Arc Current (Amp)	4	40964.00	10241.00	5.73	11.22
Electrode extension (mm)	4	28520.00	7130.00	3.99	7.81
Error	7	12509.65	1787.09		3.43
Total	19	365221.65	19222.19		100.00

Table 11: ANOVA for Impact strength

Factor	DOF	SS	MS	F	P
Gas Flow Rate (kgm/s)	4	69.27	17.32	21.04	36.99
Arc Current (Amp)	4	56.83	14.21	17.26	30.35
Electrode extension (mm)	4	55.40	13.85	16.82	29.58
Error	7	5.76	0.82		3.08
Total	19	187.26	9.86		100.00

3.3.2 Grey relational analysis

The results of the Grey Relational Analysis (GRA) applied to the experimental performance data are detailed in Tables 12–14 where the response values were normalized and converted into comparable sequences. Table 12 presents the Grey Relational Generation (GRG) values derived from the signal-to-noise ratios, Table 13 provides the Grey Relational

Coefficients (GRC) and Grey Relational Grades. The resulting factor effects for FCAW and MIGW are summarized in Tables 13 and 14, while Figures 5 and 6 display the main effect plots that reveal the optimal multi-response conditions for FCAW and MIGW, respectively.

Table 12: Results of grey relational generation for the two welding process

Seq.	FCAW			MIGW		
	GRG for Hardness	GRG for UTS	GRG for Impact energy	GRG for Hardness	GRG for UTS	GRG for Impact energy
Xo	1.000	1.000	1.000	1.000	1.000	1.000
1	0.918	0.940	0.629	0.673	0.826	1.000
2	0.741	0.732	0.582	0.441	0.650	0.034
3	0.478	0.496	1.000	0.911	0.965	0.425
4	0.945	1.000	0.567	0.787	0.881	0.867
5	0.872	0.896	0.432	0.830	0.885	0.528
6	0.864	0.877	0.779	0.869	0.940	0.425
7	0.000	0.000	0.474	0.411	0.695	0.511
8	0.919	0.977	0.427	0.915	0.947	0.432
9	0.895	0.846	0.426	0.291	0.555	0.063
10	0.457	0.482	0.000	0.000	0.000	0.278
11	0.916	0.891	0.297	1.000	1.000	0.628
12	0.914	0.889	0.616	0.959	0.978	0.725
13	0.755	0.690	0.411	0.932	0.978	0.578
14	0.622	0.582	0.629	0.910	0.961	0.357
15	0.872	0.915	0.076	0.843	0.918	0.809
16	0.505	0.448	0.284	0.876	0.942	0.000
17	0.985	0.959	0.641	0.887	0.957	0.044
18	0.753	0.633	0.530	0.964	0.979	0.479
19	1.000	0.969	0.539	0.795	0.864	0.578
20	0.920	0.919	0.128	0.857	0.905	0.754

Table 13: Results of grey relational coefficient and grades for the two welding processes

	FCAW					MIGW				
Seq	**GRC for Hardness**	**GRC for UTS**	**GRC for Impact energy**	**GR-Grade**	**GR-Grade Rank**	**GRC for Hardness**	**GRC for UTS**	**GRC for Impact energy**	**GR-Grade**	**GR-Grade Rank**
1	0.859	0.893	0.574	0.776	4	0.605	0.742	1.000	0.782	5
2	0.659	0.651	0.545	0.618	11	0.472	0.588	0.341	0.467	14
3	0.489	0.498	1.000	0.663	17	0.849	0.935	0.465	0.750	19
4	0.900	1.000	0.536	0.812	2	0.701	0.807	0.790	0.766	6
5	0.796	0.828	0.468	0.697	7	0.746	0.814	0.514	0.691	20
6	0.786	0.803	0.694	0.761	5	0.793	0.893	0.465	0.717	3
7	0.333	0.333	0.487	0.385	19	0.459	0.621	0.506	0.529	18
8	0.861	0.957	0.466	0.761	5	0.855	0.904	0.468	0.742	15
9	0.827	0.765	0.465	0.686	16	0.414	0.529	0.348	0.430	16
10	0.479	0.491	0.333	0.435	20	0.333	0.333	0.409	0.359	17
11	0.857	0.820	0.415	0.697	7	1.000	1.000	0.573	0.858	1
12	0.853	0.819	0.566	0.746	8	0.924	0.958	0.645	0.842	2
13	0.671	0.618	0.459	0.582	10	0.880	0.958	0.542	0.793	8
14	0.570	0.545	0.574	0.563	12	0.847	0.928	0.437	0.738	9
15	0.796	0.855	0.351	0.667	9	0.761	0.860	0.724	0.782	5
16	0.503	0.475	0.411	0.463	13	0.802	0.895	0.333	0.677	10
17	0.971	0.925	0.582	0.826	3	0.815	0.921	0.343	0.693	11
18	0.669	0.577	0.515	0.587	14	0.932	0.960	0.490	0.794	12
19	1.000	0.942	0.520	0.821	1	0.710	0.786	0.542	0.679	13

https://doi.org/10.4314/njt.2025.5580
http://creativecommons.org/licenses/by-nc-nd/4.0/

20	0.862	0.860	0.364	0.696	18	0.777	0.840	0.670	0.762	7

Table 14: Resulting factor effects for FCAW and MIGW

Level	Gas Flow Rate (kgm/s)		Arc Current (Amp)		Electrode extension (mm)	
	FCAW	MIGW	FCAW	MIGW	FCAW	MIGW
1	0.6857	0.4302	0.6975	**0.8578**	0.5825	**0.7933**
2	0.6300	0.6880	0.7130	0.6644	**0.7171**	0.6913
3	0.6648	**0.7619**	0.6325	0.6707	0.6623	0.6877
4	**0.7381**	0.6732	0.6551	0.6967	0.6510	0.6699
5	0.4346	0.3586	**0.7457**	0.8425	0.5627	0.7375

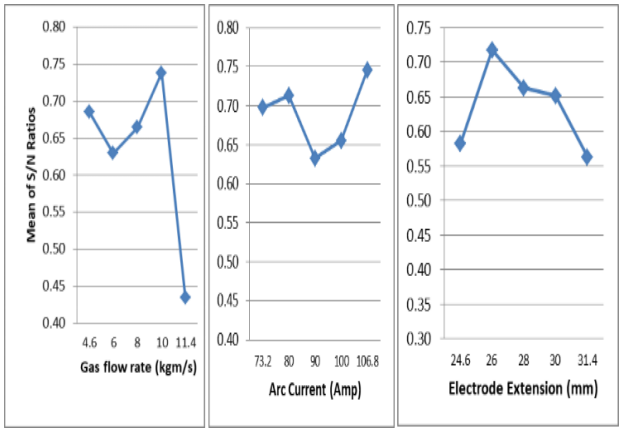

Figure 3: Main effect plots for GRA of FCAW

The highest value of Grey relational grade for FCAW and MIGW are 0.826 (run 17) and 0.858 (run 11). Adedipe *et al.* [20] have revealed that higher Grey relational grade was desired to achieve optimal performance. The data obtained from GR-Grade was used to obtain the resulting factor effects for FCAW and MIGW presented in Table 14. The values in bold represent the optimal levels of experimental factors.

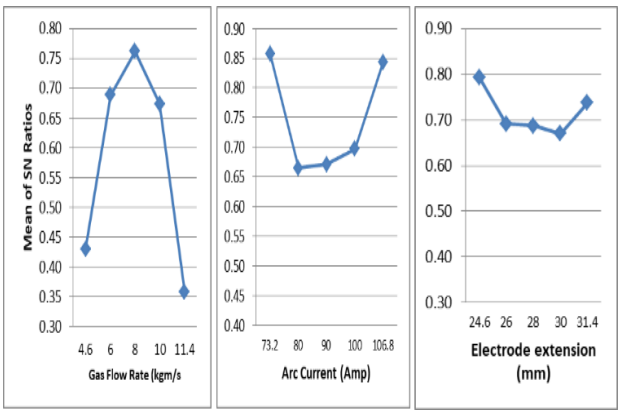

Figure 4: Main effect plots for GRA of MIGW

3.4 Microstructure of Weldment

The SEM images of the tensile test fractured surfaces for the GRA-optimized FCAW and MIGW samples (Figures 5, at 100 µm scales) revealed distinct microstructural characteristics that directly influence their mechanical properties. In the FCAW weldment (Figure 5a), the finer grain structure, uniform grain distribution, and evidence of phase transformations (ferrite and austenite) indicate a refined microstructure. Grain refinement is critical because smaller grains increase the grain boundary area [35], which impedes dislocation movement and enhances strength and toughness this explains the higher tensile and yield strengths typically observed in FCAW welds compared to MIGW. However, the presence of inclusions or slag-related features, though not compromising structural integrity, can act as stress concentrators and may slightly reduce ductility and fatigue resistance [35].

In contrast, the MIGW weldment (Figure 5b) exhibits a smoother surface finish and fewer inclusions due to the protective gas shielding, which minimizes oxidation and impurity entrapment. This cleaner microstructure contributes to improved ductility and elongation, making MIGW welds more suitable for applications requiring higher toughness and aesthetic quality. The finer grain structure in MIGW also enhances mechanical properties, but the lower inclusion content means fewer potential sites for crack initiation, resulting in better overall reliability and fatigue performance.

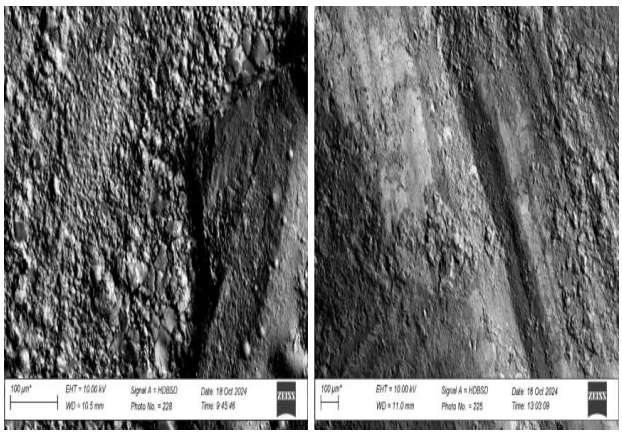

Figure 5: Microstructure of GRA-optimised (a) FCA (b) MIG weldment at 100 µm scale

Overall, the optimization of welding parameters in both processes has led to desirable microstructural features grain refinement and minimized defects which are directly responsible for the observed improvements in mechanical properties. Grain refinement increases strength and toughness, while the reduction of inclusions and porosity ensures higher ductility and fatigue resistance. These findings confirm that both FCAW and MIGW, when optimized, produce weldments with robust mechanical performance suitable for demanding engineering applications.

4.0 CONCLUSIONS

This study optimized Metal Inert Gas (MIG) and Flux Cored Arc (FCA) welding parameters for AISI 1045 alloy steel, a medium-carbon steel widely used for its strength and toughness. From the results obtained, the following conclusion can be drawn;

i. XRF identified the material as galvanized medium-carbon steel (0.376% C, 22–25% Fe), while XRD analysis revealed a crystalline structure with characteristic peaks indicating crystal size and defects.

ii. Mechanical tests showed FCAW and MIGW welds varied in hardness, UTS, and impact strength, improving with grain refinement and moderate gas flow; however, UTS remained below base metal, despite high joint efficiency.

iii. Optimal welding parameters for FCAW were 4.6 kgm/s GFR, 73.2 A, 28 mm EE (hardness) and 10 kgm/s, 73.2 A, 26 mm EE (UTS); for MIGW, 8 kgm/s, 73.2 A, 24.6 mm EE (hardness & UTS) and 6 kgm/s, 106.8 A, 26 mm EE (impact strength).

iv. ANOVA showed gas flow rate most influenced hardness and UTS in both processes; electrode extension mainly affected FCAW impact strength; errors were under 5%.

v. Microstructure analysis confirmed grain refinement and phase changes in both welds; MIG welds had smoother surfaces and fewer inclusions; no porosity or cracks were observed, highlighting the role of parameter optimization.

REFERENCES

[1] Rahadian, N. “Advancements in welding technology: A comprehensive review of techniques, materials, and applications,” *Journal PEP Bandung*, 2 (1), p. 62–110, 2025.

[2] Khan, F. Hossain, N. Mim, J. J. Rahman, S. M. Iqbal, M. J. Billah, M. and Chowdhury, M. A. “Advances of composite materials in automobile applications – A review,” *Journal of Engineering Research*, (online first), p. 1001-1023, 2024, doi: 10.1016/j.jer.2024.02.017.

[3] Kearns, W. H. Welding Handbook. Resistance of solid-state welding and other joining processes, 7th ed., Vol. 3, American Welding Society, 2020.

[4] Messler, R. W. Principle of welding processes, *Wiley–VCH Verlag GmbH & Co. KGaA*, Weinheim, 2023.

[5] Vats, V. Melton, G. Islam, M. and Krishnan, V. V. “Investigation into Cr (VI) generation in metal inert gas (MIG), metal active gas (MAG), and flux cored arc welding (FCAW) by varying the oxidation potential of the shielding gas*,” Welding in the World,* 67 (10), p. 2301–2313, 2023.

[6] Sharma, S. and Singh, L. “A review on the flux cored arc welding through process parameter,” *International Journal of Scientific Research in Mechanical and Materials Engineering*, 47, p. 777–780, 2023.

[7] Chaturvedi, M. and Vendan, S. A. Advanced welding techniques, *Springer, Berlin*, Germany, 2022.

[8] Vijayavel, P. Mahesh, G. and Venkatswarmy, M. “Optimisation of MIG welding parameters for improving strength of welding joint in AISI 10405 steel*,” International Journal of Mechanical Engineering*, 1 (2), p. 1–8, 2018.

[9] Ajit, H. Ashwari, D. and Satpal, S. “Optimisation of MIG welding process parameters to predict maximum field strength in AISI 1040*,” Industrial Journal of Mechanical Engineering*, 1 (3), p. 203-213, 2012.

[10] Raja, S. K. Balaji, N. Balasubrananian, K. and Rajendran, C. “Effect of MIG welding process parameters on microstructure and tensile behaviour of Hastelloy C276 using response surface methodology*,” International Journal of Mechanical Engineering*, 1, p. 1–7, 2019, doi: 10.1088/2053-1591/ab093a.

[11] Doniawi, A. Hassani, G. and Ranjbanj, (initials not given). "Prediction and optimisation of mechanical properties of St52 in gas metal arc weld using response surface methodology and ANOVA," *International Journal of Engineering*, 29 (9), p. 1–7, 2016.

[12] Izzatul, A. I. Ashwani, D. and Satpal, S. "Optimisation of MIG welding process parameters to predict maximum yield strength in AISI 1040," *International Journal of Mechanical Engineering and Robotics Research*, 1 (3), p. 1–11, 2012.

[13] Kashif, N. and Anwar, K. S. "Response surface methodology for FCAW for best weld condition on desirability function," *Journal of Material Sciences and Engineering*, 8 (2), p. 1–10, 2020.

[14] Rayindra, K. M. and Rajesh, K. P. "Optimisation of metal inert gas welding process during joining of structural steel," *E3S Web of Conferences*, 184, p. 01028, 2020, doi: 10.1051/e3sconf/202018401028.

[15] Madavi, K. R. Jogi, B. F. and Lohar, G. S. "Metal inert gas (MIG) welding process: A study of effect of welding parameters," *Materials Today: Proceedings*, 51, p. 690–696, 2022.

[16] Smart, S. C. "Effect of process variables on weld metal hydrogen-assisted cold cracking in multipass welds of high strength steels," *Ph.D. dissertation*, University of Leicester, 2024.

[17] Abutu, J. Lawal, S. A. Ndaliman, M. B. Lafia-Araga, R. A. Adedipe, O. and Choudhury, I. A. "Production and characterization of brake pad developed from coconut shell reinforcement material using central composite design," *SN Applied Sciences*, 1 (18), p. 1–16, 2019.

[18] Irechukwu, C. C. Khan, R. H. Abutu, J. Lawal, S. A. and Namessan, N. O. "Effect of tungsten inert gas welding parameters on the performance of AISI 304 alloy steel using multi-response optimisation technique," *Welding International,* 35 (1–3), p. 45–58, 2021.

[19] Benyounis, K. Y. and Olabi, A. G. "Optimisation of different welding processes using statistical and numerical approaches – A reference guide," *Advances in Engineering Software*, 39 (6), p. 483–496, 2008.

[20] Adedipe, O. Gambo, A. B. Abutu, J. Olugboji, O. A. Agboola, J. B. Obanimomo, K. T. and Abdulrahman, A. S. "An evaluation of mechanical properties and estimation of environmental reduction factors in welded API X70 steel pipeline in natural seawater," *Welding International*, 37 (5), p. 269–281, 2023.

[21] Singh, S. Samir, S. Kumar, K. and Thapa, S. "Effect of heat treatment processes on the mechanical properties of AISI 1045 steel," *Materials Today: Proceedings*, 45, p. 5097–5101, 2021.

[22] Hossain, M. S. Shaikh, M. A. A. Rahaman, M. S. and Ahmed, S. "Modification of the crystallographic parameters in a biomaterial employing a series of gamma radiation doses," *Molecular Systems Design & Engineering*, 7 (10), p. 1239–1248, 2022.

[23] Salem, K. S. Kasera, N. K. Rahman, M. A. Jameel, H. Habibi, Y. Eichhorn, S. J. … and Lucia, L. A. "Comparison and assessment of methods for cellulose crystallinity determination," *Chemical Society Reviews,* 52 (18), p. 6417–6446, 2023.

[24] Igwe, N. C. Akhrif, I. and El Jai, M. "On the machinability of additively manufactured AlSi10Mg: factorial analysis and multi-objective optimization," *International Journal on Interactive Design and Manufacturing (IJIDeM)*, p. 1–42, 2025.

[25] Igwe, N. C. Igwe, A. C. Ononiwu, N. H. Ozoegwu, C. G. Akhrif, I. and El Jai, M. "Taguchi-grey relational optimization of surface roughness and tool wear in turning of rice husk ash reinforced aluminum," *Moroccan Journal of Chemistry*, 13 (3), p. JChem–??, 2025.

[26] Igwe, N. C. Akhrif, I. El Jai, M. and El Fahime, B. "An experimental investigation of the influence of SLM input factors on the as-built AlSi10Mg surface quality," *The International Journal of Advanced Manufacturing Technology*, 136 (2), p. 619–674, 2025.

[27] Igwe, N. C. Salim, R. Ech-chihbi, E. Akhrif, I. El Jai, M. and Hammouti, B. "The influence of laser powder bed fusion process parameters on the corrosion behavior of AlSi10Mg alloy in NaCl solution," *The International Journal of Advanced Manufacturing Technology*, p. 1–10, 2025.

[28] Van, A. L. Truong-An, N. Trung-Thanh, N. and Dang, X. B. "Multi-performance

optimization of gas metal arc welding operation in terms of energy saving and quality criteria," *Journal of Adhesion Science and Technology*, 39 (1), p. 76–105, 2025.

[29] Lawong, A. Nampromma, S. Sudsuansee, T. and Sergsiri, S. "Multi-response optimization of robotic welding parameters using a Taguchi-based random forest model for dissimilar joining materials," *Engineering, Technology & Applied Science Research*, 15 (5), p. 27237–27243, 2025.

[30] Jawad, M. Jahanzaib, M. Ali, M. A. Farooq, M. U. Mufti, N. A. Pruncu, C. I. Salman, H. and Wasim, A. "Revealing the microstructure and mechanical attributes of pre-heated conditions for gas tungsten arc welded AISI 1045 steel joints," *International Journal of Pressure Vessels and Piping*, 192, p. 104440, 2021.

[31] Marimuthu, P. K. Sri Kurumurthy, G. Thenarasu, M. and Venkata Roshan, M. "Minimizing residual stresses in AISI 1045 steel through optimization of cutting parameters: A particle swarm optimization approach," Proceedings of the Institution of Mechanical Engineers, *Part E: Journal of Process Mechanical Engineering*, p. 09544089251318779, 2024.

[32] Şeker, A. Değirmencioğlu, F. and Karakuş, M. "Investigation of the effects of shielding gas flow rate on weld penetration in MIG welding," *Journal of Materials and Manufacturing (J. Mater. Manuf.)*, 2 (2), p. 28–37, 2023.

[33] Abd Rahman, M. N. Zulkipli, N. H. Kasim, M. S. Jamli, M. R. and Budi, E. "Impact of argon gas shielding flow rate on the hardness of weld joint," *Journal of Advanced Manufacturing Technology*, 16 (1), p. 1–10, 2022.

[34] Li, T. Zhang, Y. Gao, L. and Zhang, Y. "Optimization of FCAW parameters for ferrite content in 2205 DSS welds based on the Taguchi design method," *Advances in Materials Science and Engineering*, 2018 (1), p. 7950607, 2018.

[35] Liang, Z. Li, H. Wang, Q. Sun, X. Gao, X. Yuan, S., Yang, Z and Zhang, F. "Enhancing the resistance to hydrogen embrittlement in bainitic steel via grain refinement, dislocation density reduction, and retained austenite stability improvement," *Journal of Materials Science & Technology*, 247, p. 214–225, 2026.

[36] Shuvo, M. M. "Improving sustainability of sand-casting processes via novel 3D mold designs," *Ph.D. dissertation*, Pennsylvania State University, 2023

https://doi.org/10.4314/njt.2025.5580